JGR Oceans

RESEARCH ARTICLE
10.1029/2023JC020436

Mississippi River Chemistry Impacts on the Interannual Variability of Aragonite Saturation State in the Northern Gulf of Mexico

Fabian A. Gomez[1,2], Rik Wanninkhof[2], Leticia Barbero[2,3], and Sang-Ki Lee[2]

[1]Northern Gulf Institute, Mississippi State University, Starkville, MS, USA, [2]NOAA Atlantic Oceanographic and Meteorological Laboratory, Miami, FL, USA, [3]Cooperative Institute for Marine and Atmospheric Studies, University of Miami, Miami, FL, USA

Key Points:

- We simulated the Mississippi River impacts on interannual patterns of aragonite saturation (Ω_{Ar}) in the northern Gulf of Mexico
- High-discharge conditions increase the frequency of suboptimal Ω_{Ar} levels for coastal calcifying species in all seasons
- Reduced Ω_{Ar} under high-discharge is linked to low buffer capacity of riverine water in winter and enhanced bottom remineralization in summer

Supporting Information:

Supporting Information may be found in the online version of this article.

Correspondence to:

F. A. Gomez,
fabian.gomez@noaa.gov

Citation:

Gomez, F. A., Wanninkhof, R., Barbero, L., & Lee, S.-K. (2024). Mississippi River chemistry impacts on the interannual variability of aragonite saturation state in the Northern Gulf of Mexico. *Journal of Geophysical Research: Oceans*, *129*, e2023JC020436. https://doi.org/10.1029/2023JC020436

Received 3 SEP 2023
Accepted 26 JAN 2024

Abstract In the northern Gulf of Mexico shelf, the Mississippi-Atchafalaya River System (MARS) impacts the carbonate system by delivering freshwater with a distinct seasonal pattern in both total alkalinity (Alk) and dissolved inorganic carbon (DIC), and promoting biologically driven changes in DIC through nutrient inputs. However, how and to what degree these processes modulate the interannual variability in calcium carbonate solubility have been poorly documented. Here, we use an ocean-biogeochemical model to investigate the impact of MARS's discharge and chemistry on interannual anomalies of aragonite saturation state (Ω_{Ar}). Based on model results, we show that the enhanced mixing of riverine waters with a low buffer capacity (low Alk-to-DIC ratio) during high-discharge winters promotes a significant Ω_{Ar} decline over the inner-shelf. We also show that increased nutrient runoff and vertical stratification during high-discharge summers promotes strong negative anomalies in bottom Ω_{Ar}, and less intense but significant positive anomalies in surface Ω_{Ar}. Therefore, increased MARS discharge promotes an increased frequency of suboptimal Ω_{Ar} levels for nearshore coastal calcifying species. Additional sensitivity experiments further show that reductions in the Alk-to-DIC ratio and nitrate concentration from the MARS significantly modify the simulated interannual Ω_{Ar} patterns, weakening the positive surface Ω_{Ar} anomalies during high-discharge summers or even producing negative surface Ω_{Ar} anomalies. Our findings suggest that riverine water carbonate chemistry is a main driver of interannual variability in Ω_{Ar} over river dominated ocean margins.

Plain Language Summary The Mississippi river strongly impacts seawater chemistry and biological production over the northern Gulf of Mexico, leading to changes in ocean acidification. An increased acidity is concurrent with increased solubility in calcium carbonate ($CaCO_3$), which has the potential to negatively impact calcifying organisms that build-up hard structures of this mineral compound, like shellfish and corals. Near-corrosive acidic conditions for $CaCO_3$ have been documented in the proximity of the Mississippi delta during summer, but it is not well known how changes in the Mississippi river discharge and chemistry influence the year-to-year changes in $CaCO_3$ solubility. Here we use a numerical model that realistically simulates oceanic and biogeochemical dynamics to investigate this aspect. Our model identifies seasonal distinctive mechanisms leading to increased $CaCO_3$ solubility nearshore, mainly driven by the mixing of relatively more acidic Mississippi river waters (compared to seawater) during high-discharge winters, and biological processes stimulated by riverine nutrients during high-discharge summers. The increased $CaCO_3$ solubility in high-discharge years promotes suboptimal conditions for the growth of calcifying organisms, and the opposite is true in low-discharge years. Our study highlights that river discharge, river acidity, and river nutrient concentrations are key variables modulating the interannual $CaCO_3$ solubility patterns in river-influenced coastal margins.

1. Introduction

Ocean Acidification (OA), caused by the ocean uptake of anthropogenic atmospheric carbon dioxide (CO_2), is leading to a sustained decline in ocean pH, along with an increase in partial pressure of CO_2 (pCO_2) and calcium carbonate solubility (Doney et al., 2009; Gruber et al., 2019). These changes are exerting significant stress on marine species and ecosystems, including negative impacts on growth and survival of calcifying organisms (e.g., Orr et al., 2005). The rate of OA progression has significant spatial variability over continental margins, where processes such as coastal upwelling, horizontal and vertical mixing, and river runoff can strongly influence carbonate chemistry patterns (e.g., Duarte et al., 2013). In particular, rivers play a relevant role, as they transport large amounts of freshwater, nutrients, carbon, and alkalinity that affect inorganic carbon distribution and coastal

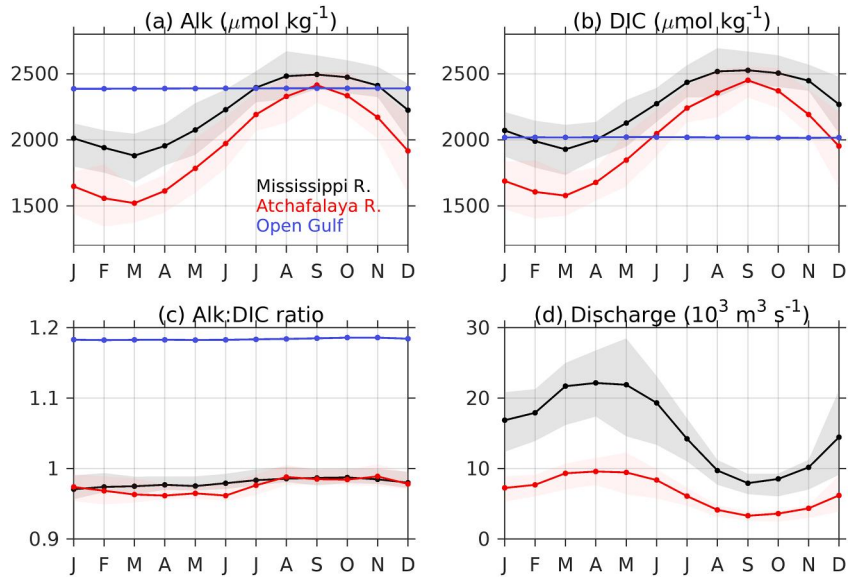

Figure 1. MARS monthly climatologies during 1980–2019: (a) alkalinity (Alk), (b) dissolved inorganic carbon (DIC), (c) alkalinity-to-DIC ratio (Alk:DIC ratio), and (d) discharge for the Mississippi (black) and Atchafalaya (red) rivers. Interquartile intervals are also depicted as gray and light red shadows, respectively. Simulated surface alkalinity, DIC, and Alk:DIC ratio over open Gulf waters are shown in blue for comparison with river patterns.

acidity (e.g., Lacroix et al., 2020, 2021; Liu et al., 2021; Regnier et al., 2022). Understanding and constraining this river-induced variability is needed to properly evaluate marine ecosystem vulnerability to OA progression.

The northern Gulf of Mexico (GoM) shelf is a river-dominated ocean margin, strongly impacted by river runoff from the Mississippi-Atchafalaya River System (MARS). The nutrient delivery from the MARS promotes enhanced phytoplankton production in the surface ocean layer over the Louisiana-Texas shelf, which contributes to reducing dissolved inorganic carbon (DIC), increasing pH, and decreasing pCO_2, the latter favoring an enhanced uptake of atmospheric CO_2 (Huang et al., 2015; Lohrenz & Cai, 2006). The associated export of organic carbon to the bottom layer and its remineralization decreases dissolved oxygen (DO) and releases CO_2, promoting bottom hypoxia and acidification during summer, when a strong stratification prevents vertical mixing of the whole water column (Cai et al., 2011; Rabalais et al., 2007). Besides these biologically induced changes, the MARS has relatively high concentrations of total alkalinity (Alk) and DIC compared to other rivers in the United States (Gomez et al., 2023), which further influences ocean carbonate patterns. For example, high salinity-normalized alkalinity in the northern GoM has been connected to the mixing of alkalinity-rich waters from the MARS (Yang et al., 2015). However, an integrated description of the MARS's carbonate chemistry impacts on the coastal ecosystem has remained relatively overlooked. Particularly, it is not well known how temporal changes in river Alk and river DIC impact the buffer capacity nearshore. This could be a relevant aspect considering that Alk and DIC from the MARS have a strong seasonal variability. Indeed, the annual amplitude for these two variables is about 600 and 800 μmol kg^{-1} for the Mississippi and Atchafalaya Rivers, respectively, which is substantially larger than the seasonal variability in open ocean waters (Figures 1a and 1b).

Changes in pH, pCO_2, and aragonite saturation state (Ω_{Ar}), three regularly used OA metrics, are driven by changes in temperature, salinity, Alk, and DIC. Ω_{Ar} represents the solubility of aragonite, a specific mineral phase of $CaCO_3$, which can be defined by:

$$\Omega_{Ar} = \left[CO_3^{2-}\right] \cdot \left[Ca^{2+}\right] \cdot K_{Ar}^{-1} \quad (1)$$

where $\left[CO_3^{2-}\right]$ is the carbonate ion concentration, a property strongly correlated to the Alk-to-DIC ratio (Alk:DIC ratio), $[Ca^{2+}]$ is the calcium ion concentration, which varies with salinity, and K_{Ar} is the apparent solubility product of aragonite, a function of temperature, salinity, and pressure (Wang et al., 2013; Wanninkhof et al., 2015). Aragonite is prone to dissolve at Ω_{Ar} values lower than one, but calcifying organisms may start

experiencing stress under Ω_{Ar} values lower than 2.0 (e.g., Kekuewa et al., 2022; Siedlecki et al., 2021). Quantifying the occurrence of those suboptimal levels ($\Omega_{Ar} < 2.0$) is therefore relevant for the management of shellfish and other important marine resources, such as the oyster *Crassotea virginia*, an important fishery resource along the northern GoM coast (Turner, 2006). Previous studies have reported a marked decline in bottom Ω_{Ar} near the MARS delta during summer, concurrent with bottom hypoxia (Cai et al., 2011; Laurent et al., 2017). However, year-to-year changes in coastal Ω_{Ar} patterns have been poorly described, and relationships linking MARS discharge to Ω_{Ar} anomalies have not been yet established. As such, coastal ecosystem vulnerability to suboptimal Ω_{Ar} conditions in the region remains uncertain.

Further understanding of the carbonate system responses to changes in river runoff is important to assess regional vulnerabilities to OA. To this goal, high-resolution ocean biogeochemical (BGC) models that simulate carbon dynamics can provide valuable insights. In the present study we used outputs from an ocean-BGC model configured by Gomez et al. (2020) to examine the carbonate system response to changes in MARS discharge and chemistry. To this effect, we characterize the simulated interannual anomaly patterns for salinity, Alk, DIC, and Ω_{Ar} during high and low MARS discharge periods, identifying the main underlying factors modulating those anomalies. We then performed a sensitivity analysis to investigate to what degree changes in MARS chemistry could modify the link between MARS discharge and interannual Ω_{Ar} variability. Finally, we derived frequency histograms for Ω_{Ar} under high and low MARS discharge conditions, quantifying the fraction of suboptimal Ω_{Ar} levels for calcifying organisms.

2. Materials and Methods

The ocean-biogeochemical model, referred to as GoMBio, simulates 16 state variables, including Alk and DIC. It was built up in the Regional Ocean Model System (ROMS; Shchepetkin & McWilliams, 2005), with a horizontal resolution of 8 km and 37 sigma-coordinate vertical levels. Initial and open boundary conditions were derived from a 25 km horizontal resolution model for the North Atlantic (Liu et al., 2015). Surface fluxes of momentum, heat, and freshwater were derived from the ERA5 reanalysis product (Hersbach et al., 2020) using bulk flux parameterizations. Daily river discharge for U.S. rivers was obtained from the U.S. Army Corps of Engineers and U.S. Geological Survey (USGS) records, available at the Gulf of Mexico Coastal Ocean Observing System (https://geo.gcoos.org/river_discharge/). River chemistry for U.S. rivers was obtained from RC4USCoast (Gomez et al., 2023), a river chemistry data set based on the USGS Water Quality Database. Discharge and chemistry data for Mexican rivers were derived from the scientific literature (e.g., Martínez-López & Zavala-Hidalgo, 2009; Muñoz-Salinas & Castillo, 2015). Further model details can be found in Gomez et al. (2020). The Ω_{Ar} outputs were derived offline from the simulated monthly outputs of Alk, DIC, temperature, and salinity. To this effect, we used the MatLab version of the CO2SYS program for CO_2 System Calculations (van Heuven et al., 2011), considering the CO_2 solubility constant from Weiss (1974), the carbonic acid dissociation constants of Millero (2010), and the boric acid dissociation constant of Dickson (1990).

To investigate the impact of interannual changes in MARS runoff on the carbonate system variability, we conducted a composite analysis of the mean detrended anomalies of salinity, DIC, Alk, and Ω_{Ar} during high and low discharge conditions (hereinafter anomaly implies a monthly model output with the monthly climatology average subtracted). Patterns were estimated for the model surface and bottom layers, which have an average thickness of 0.5 and 4.9 m over the northern Gulf shelf, respectively. To account for seasonal variation in the carbonate system response to runoff changes, independent composites were generated for winter (December–February), spring (March–May), summer (June–August), and fall (September–November). The percentiles 75% and 25% of seasonal averaged MARS discharge series were used as thresholds to define high and low discharge periods, respectively. The seasonally averaged discharge series were derived from daily discharge observations, and led the anomaly composite for 1-week to account for a lagged phytoplankton response to runoff changes. For example, the winter averaged discharge series integrated observations from the last week of November to the third week of February. The selected composite's years for each season (10 years) are reported in Table S1 in Supporting Information S1. The statistical significance of the composites was assessed with Monte Carlo experiments (von Storch and Zwiers, 1999). For each variable, 1,000 independent realizations of the composite were generated by randomly selecting 10 years from 1980 to 2019. A composite anomaly was significant at the 90% level when it fell outside the interval defined by the percentiles of 5% and 95% from the randomly generated composite distribution.

To investigate the role of Alk, DIC, salinity (S), and temperature (T) as main underlying drivers of Ω_{Ar} variability, we performed a first order Taylor series decomposition:

$$\Delta\Omega_{Ar} \approx \frac{\partial\Omega_{Ar}}{\partial Alk}\cdot\Delta Alk + \frac{\partial\Omega_{Ar}}{\partial DIC}\cdot\Delta DIC + \frac{\partial\Omega_{Ar}}{\partial S}\cdot\Delta S + \frac{\partial\Omega_{Ar}}{\partial T}\cdot\Delta T \quad (2)$$

Where $\Delta\Omega_{Ar}$ represents the temporal change for Ω_{Ar}, and the four right side terms in Equation 2 represent the Alk, DIC, salinity and temperature contribution to the Ω_{Ar} change, respectively. The partial derivatives of the contribution terms were calculated by adding a small perturbation (0.0001 in magnitude) to each driver while keeping the other three terms as constant, using the CO2SYS program.

In addition to the model hindcast, we conducted five experiments to evaluate the carbonate system sensitivity to changes in MARS chemistry (Table S2 in Supporting Information S1). In the Constant Carbonate (CCBN) experiment, we used long-term (1980–2019) averages for the Mississippi and Atchafalaya Alk (1,956 and 2,215 μmol kg^{-1}, respectively) and DIC (2,002 and 2,258 μmol kg^{-1}, respectively) instead of time evolving patterns. Thus, in this simulation, we removed the seasonal, interannual, and long-term variability from the river Alk and DIC concentrations. In the Alk090 and Alk110 experiments, the MARS's Alk was reduced and increased by 10%, respectively (i.e., an average Alk increase/decrease of about 196 mmol kg^{-1} for the Atchafalaya River, and 222 mmol kg^{-1} for the Mississippi River). Finally, in the N80 and N50, the MARS's nitrate concentration (about 83 μmol kg^{-1} during 1980–2019) was decreased by 20% and 50%, respectively. N50 represents an important decrease in nitrate concentration (about 40 mmol kg^{-1}), which could be connected to the nitrogen load reduction target of 45% set by the Hypoxia Task Force to mitigate bottom hypoxia (www.epa.gov/ms-htf; last access: September 2023).

3. Results

3.1. Composite Analysis

Figure 2 shows the surface and bottom composites for salinity, Alk, and DIC under high MARS discharge conditions. The salinity patterns revealed a significant coastal freshening, which was mostly constrained to the inner-shelf (bottom depth <25 m), with surface and bottom salinity (SSS and *b*Sal) anomalies reaching magnitudes greater than 1.5 and 0.5, respectively, near the MARS delta (Figures 2a and 2d). The coastal freshening was concurrent with a significant decrease in surface and bottom Alk (*sf*Alk and *b*Alk) during winter-spring, with the largest anomaly magnitude exceeding 40 and 20 μmol kg^{-1}, respectively (Figures 2b and 2e). In contrast, the Alk anomalies were mostly not significant during summer-fall (Figures 2b and 2e). To some degree, the surface DIC (*sf*DIC) pattern resembled that for *sf*Alk (Figure 2c), but with weaker anomalies in winter-spring, and significant positive anomalies near the Mississippi mouth in summer-fall (>30 μmol kg^{-1}; Figure 2c). On the other hand, the bottom DIC (*b*DIC) patterns largely differed from the *b*Alk pattern, showing significant positive anomalies during summer-fall, which exceeded 30 μmol kg^{-1} near the delta (Figure 2f).

The significant *sf*Alk decline during high discharge winters and springs can be linked to a strong MARS dilution effect on Alk, as the MARS' Alk was substantially lower than the open ocean Alk (<2,000 μmol kg^{-1}). This was connected with a flow-dependent seasonal variability in river alkalinity, which displayed a minimum in late-winter and early spring (Figures 1a and 1d), and a negative correlation between discharge and river alkalinity at the interannual timescale, which was especially strong during winter ($r = -0.65$; Figure 3). Similarly, the *sf*DIC anomalies during high discharge conditions were influenced by seasonal and interannual changes in MARS's DIC (Figures 1b and 3), which promoted a prevailing dilution effect during winter-spring (but weaker compared to that for *sf*Alk), and an enrichment effect during summer-fall. On top of this variability, an enhanced biological uptake of DIC, reflected in positive surface net community production (NCP, which is the difference between primary production and respiration) and dissolved oxygen (produced by photosynthesis) anomalies (Figures 4a and 4b), contributed to reinforce the river dilution signal in winter-spring, and counteract the river enrichment in summer-fall (more details in Section 3.2). *sf*DIC was further impacted by changes in air-sea CO_2 fluxes, with an increased outgassing near Mississippi and Atchafalaya mouths, and carbon uptake over part of the inner-shelf (Figure 4c). However, the changes in the magnitude of the air-sea CO_2 fluxes were relatively small compared to the biologically induced changes. Indeed, over the inner-shelf between 93° and 89°W (hereinafter referred to as the central inner-shelf), the median surface NCP and CO_2 flux anomalies were 8.1 and

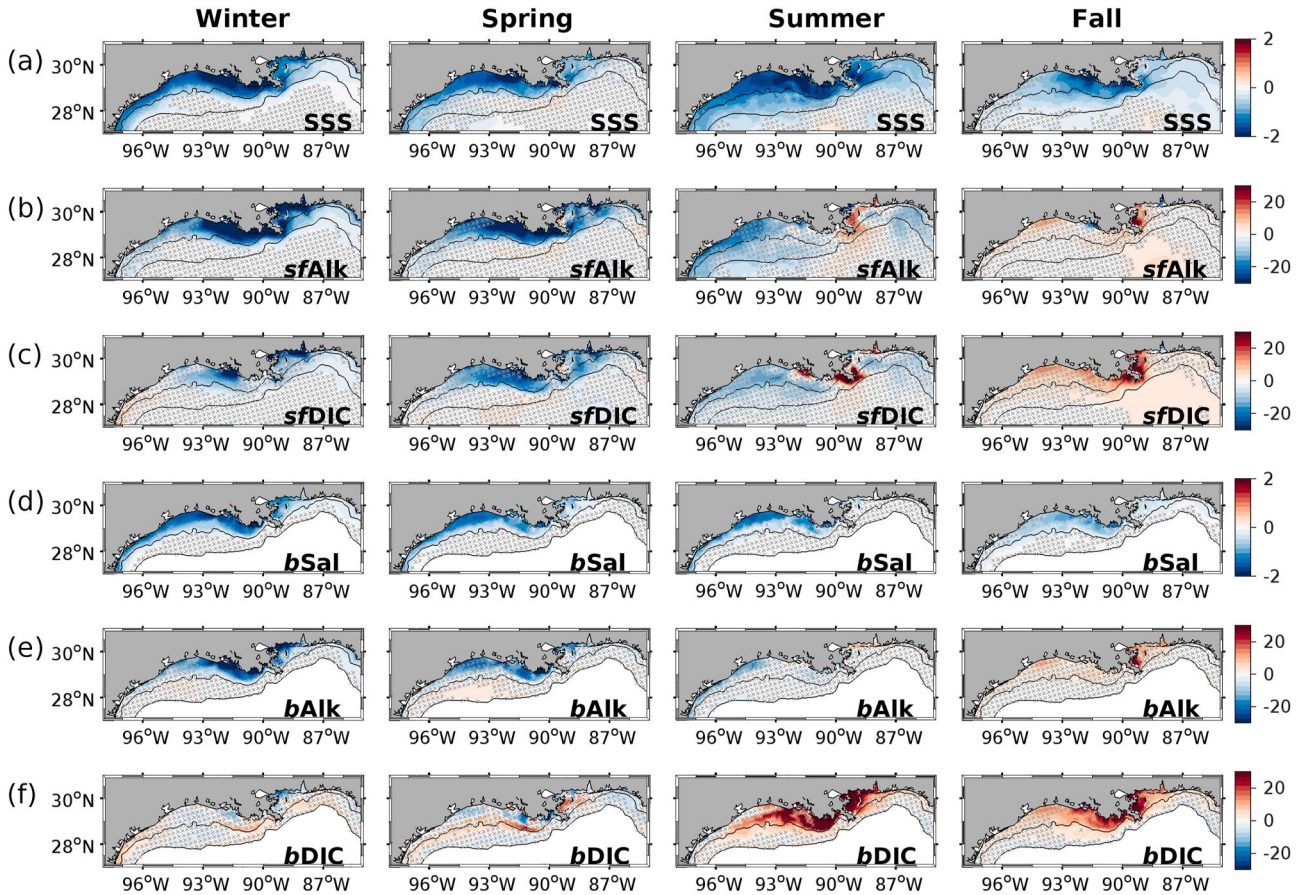

Figure 2. High discharge composites of the hindcast anomalies of (a) sea surface salinity (SSS), (b) surface alkalinity (*sf*Alk), (c) surface DIC (*sf*DIC), (d) bottom salinity (*b*Sal), (e) bottom alkalinity (*b*Alk), and (f) bottom DIC (*b*DIC) during winter, spring, summer, and fall. Anomaly series were detrended before estimating the composites. Black contours depict the 25 and 200 m isobaths. Alkalinity and DIC anomalies are in μmol kg^{-1}. Gray slash pattern represents non-significant values.

-1.6 mmol m^3 day^{-1}, respectively. High discharge conditions also promoted respiration leading to negative bottom NCP and dissolved oxygen anomalies, reflecting increased bottom remineralization in the four seasons (Figures 4d and 4e). During summer, the strong bottom oxygen decrease mirrors the strong *b*DIC increases (Figures 2f and 4e), indicative of increased bottom acidification due to strong vertical stratification.

The surface Ω_{Ar} ($sf\Omega_{Ar}$) response to the MARS-induced changes in SSS, *sf*Alk, and *sf*DIC displayed an important seasonal modulation (Figure 5a). Strong negative anomalies (>0.3 units) prevailed over the inner-shelf during winter, while positive anomalies (>0.1 units) dominated in part of the inner and outer shelf during summer. Strong negative anomalies also were found near the Mississippi and Atchafalaya River mouths during spring-fall (>0.3 units). Since $sf\Omega_{Ar}$ near the delta is the lowest in winter and highest in summer (Figure S1a in Supporting Information S1), the derived anomaly patterns imply a strengthening of both the seasonal minimum in winter and the seasonal maximum in summer. The Taylor series decomposition (Equation 2) showed that the $sf\Omega_{Ar}$ composite's anomalies were mainly determined by a balance between Alk- and DIC-induced changes (Figures 5b–5e). During winter, the mean Alk-induced change on Ω_{Ar} was -0.46 over the central inner-shelf, 2.5 times greater than the mean DIC-induced change, leading to the significant $sf\Omega_{Ar}$ drop. During summer, the DIC-induced changes prevailed over 93°–89°W, leading to negative anomalies near the Mississippi and Atchafalaya mouths, and positive anomalies further away from the discharge points. Surface freshening had a relatively weak positive impact on $sf\Omega_{Ar}$ (0.04 on average) contributing to attenuate the $sf\Omega_{Ar}$ decline in winter, and accentuate the $sf\Omega_{Ar}$ increase in summer. Temperature driven changes were small (0.002 on average) and did not contribute significantly to the total anomaly (not shown). In the bottom layer, the composite showed significant Ω_{Ar} decline over the inner-shelf in the four seasons (Figure 6a), with the strongest anomalies in summer (>0.3 units). As bottom Ω_{Ar} ($b\Omega_{Ar}$) near the delta is the lowest in summer (Figure S1b in Supporting Information S1), the pattern implies a

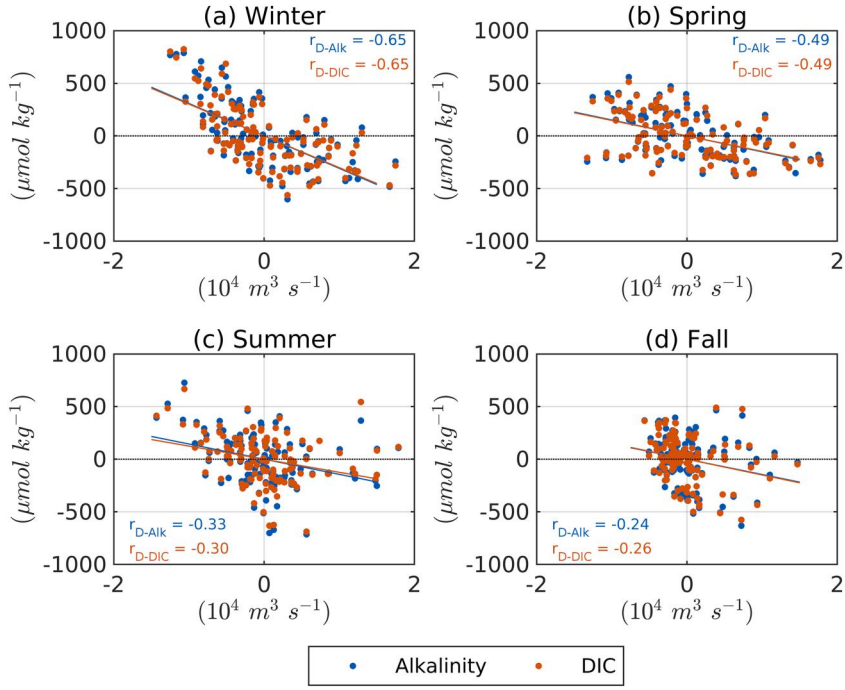

Figure 3. Mississippi River's anomalies of alkalinity and DIC against discharge anomalies. Patterns were derived from monthly averaged records during 1980–2019. Correlation coefficients between discharge and both alkalinity ($r_{D\text{-}Alk}$) and DIC ($r_{D\text{-}DIC}$) anomalies are indicated at each panel.

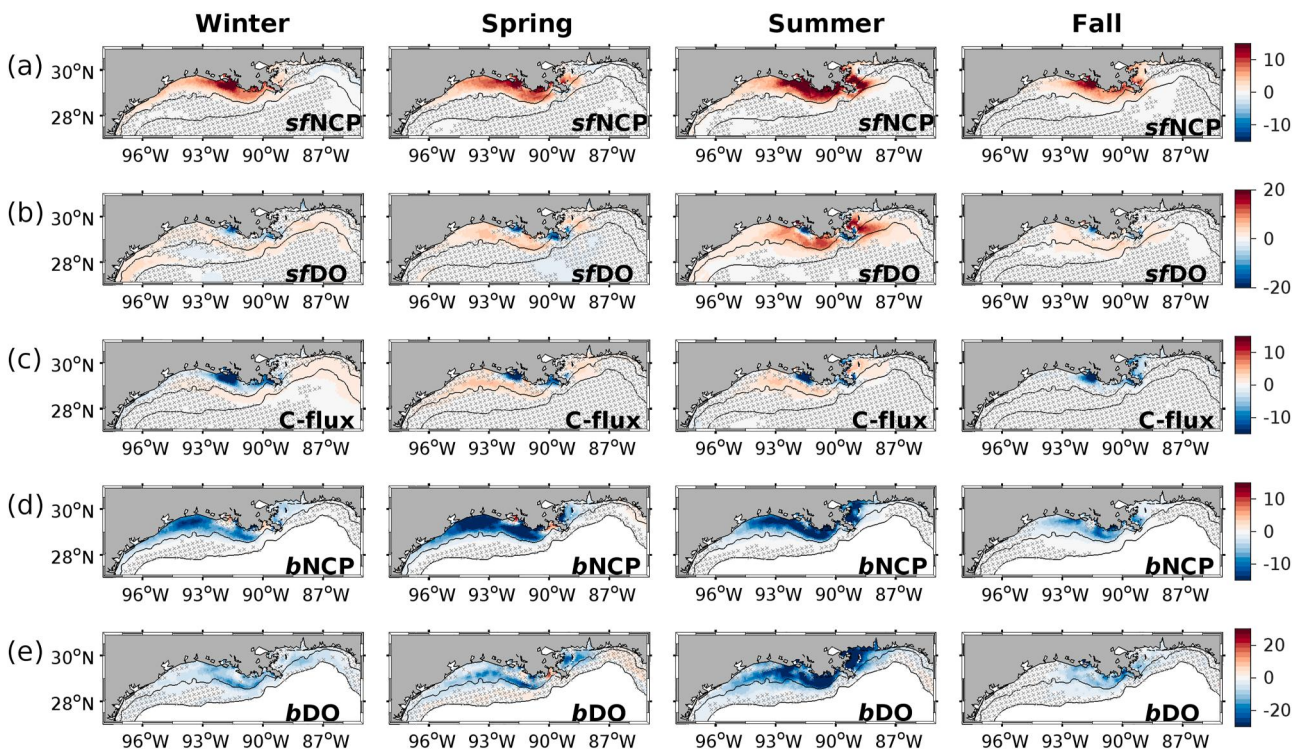

Figure 4. High discharge composites of the hindcast anomalies of (a) surface net community production (*sf*NCP), (b) surface dissolved oxygen (*sf*DO), (c) air-sea CO_2 flux (C-flux), (d) bottom net community production (*b*NCP), and € bottom dissolved oxygen (*b*DO) € during winter, spring, summer, and fall. Anomaly series were detrended before estimating the composites. Black contours depict the 25 and 200 m isobaths. Anomalies are in mmol m^{-3} day^{-1} for NCP and C-flux, and µmol kg^{-1} for DO. Negative C-flux anomalies imply decreased carbon uptake or enhanced carbon outgassing. Gray slash pattern represents non-significant values.

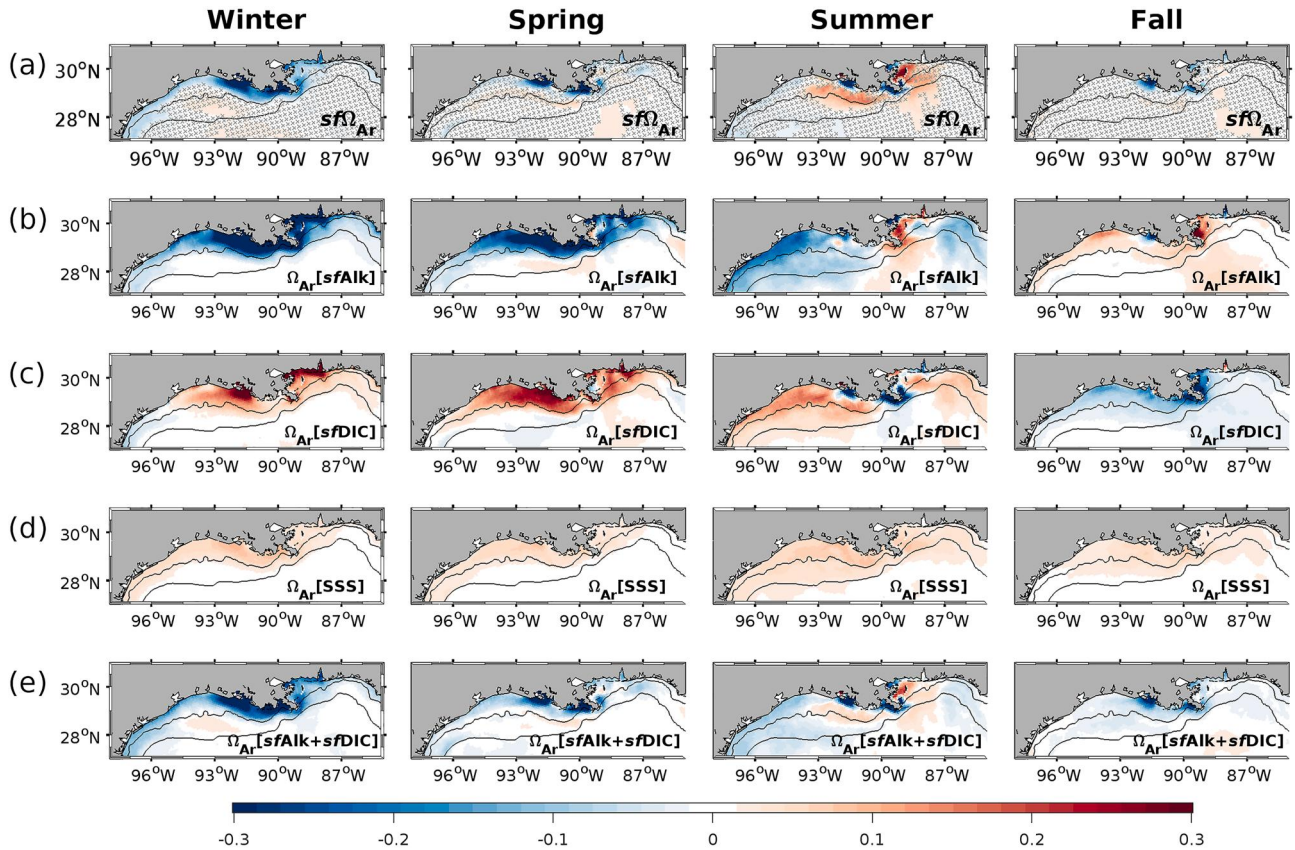

Figure 5. (a) High discharge composites of surface aragonite saturation during winters, springs, summers, and falls, as derived from the model hindcast; (b–e) Taylor decomposition terms of the composite's patterns, representing changes induced by (b) surface alkalinity (sAlk), (c) surface DIC, (d) sea surface salinity (SSS), and (e) the added effect of sAlk and sDIC. The temperature term was omitted since it has a residual impact in the composite. Anomaly series were detrended before estimating the composites. Dotted area in (a) represents non-significant anomalies. Black contours depict the 25 and 200 m isobaths.

more pronounced seasonal minimum during high-discharge summers. The Taylor decomposition for the bottom Ω_{Ar} anomalies indicated that changes in Alk in winter-spring, and DIC in summer-fall, led to those anomaly patterns (Figures 6b–6e).

The carbonate system patterns during low discharge conditions were mostly opposite to those in the high discharge scenarios (Figures S2–S5 in Supporting Information S1). Significant positive anomalies were obtained for *sf*Alk, *sf*DIC, and *b*Alk during winter-summer, and significant negative anomalies for *b*DIC during summer. Besides, $sf\Omega_{Ar}$ showed prevailing positive anomalies in the inner-shelf during winter-spring, and a significant $sf\Omega_{Ar}$ decline in part of the inner and outer shelf during summer. Finally, the $b\Omega_{Ar}$ anomalies showed significant positive values in the four seasons, with a maximum in summer.

3.2. Sensitivity Analysis

The high discharge composites for Alk and DIC in the Constant Carbonate experiment (CCBN; Table S2 in Supporting Information S1) showed important differences with respect to the hindcast's composites (Figure S6 in Supporting Information S1). During winter-spring, the CCBN experiment produced negative *sf*Alk and *b*Alk anomalies over the central inner-shelf that were on average 20 and 10 µmol kg^{-1} smaller than those in the hindcast experiment (64% and 69% decrease in magnitude), respectively, and, unlike the hindcast, displayed positive *sf*DIC anomalies near the rivers' mouths and positive *b*DIC anomalies over the inner-shelf. Also, during summer-fall, the positive *sf*DIC anomalies near the river's mouths decreased by 20–30 µmol kg^{-1}. Despite all those changes, the Ω_{Ar} anomalies for the CCBN experiment closely resembled those in the hindcast experiment (Figures 7a and 7b and Figures S7a and S7b in Supporting Information S1). An examination of the Alk:DIC ratio from MARS waters provides insight to explain the Ω_{Ar} pattern similarities. The Mississippi and Atchafalaya

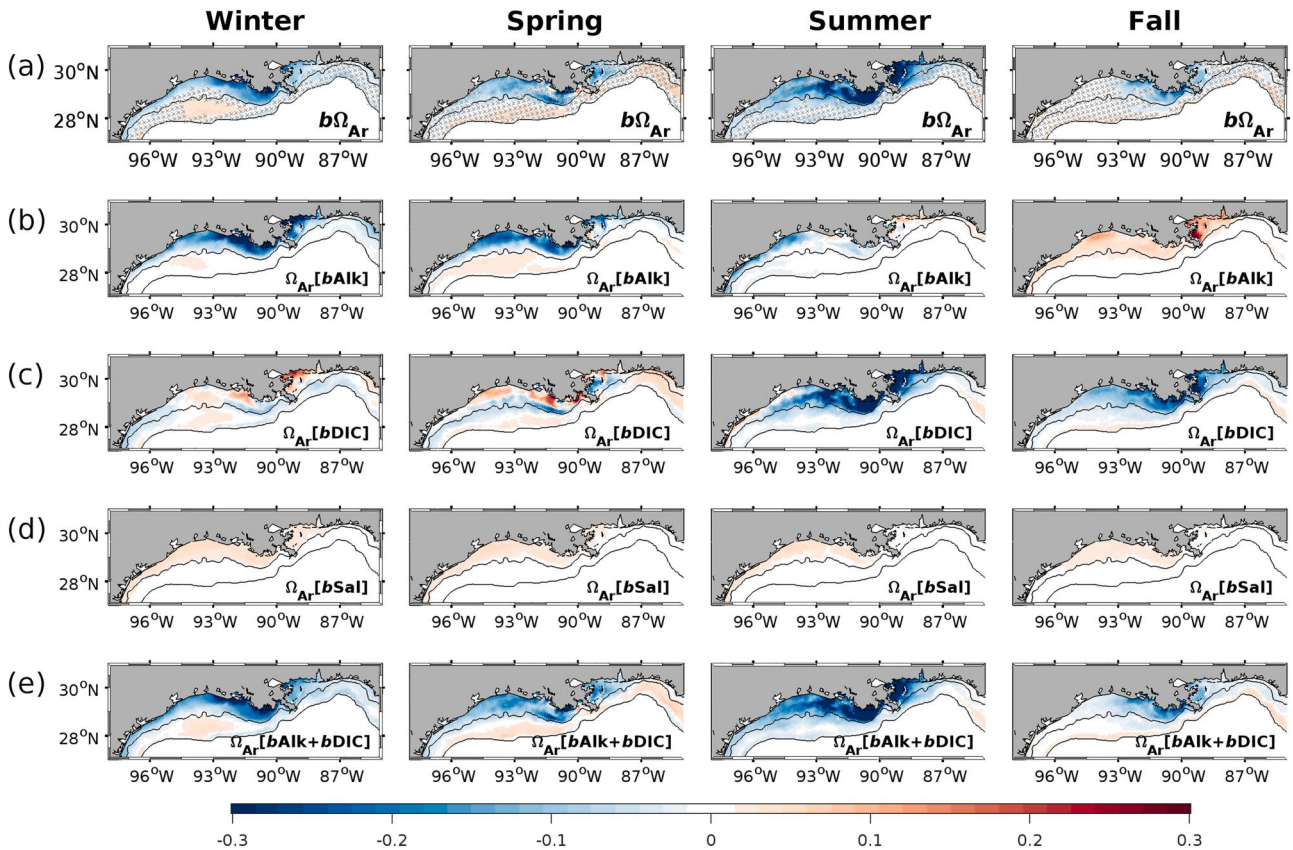

Figure 6. As Figure 5 but for bottom aragonite saturation state.

Rivers are characterized by a strong seasonal variation in Alk and DIC, but the ratio between these two variables has a weak annual variation, with an average and standard deviation of about 0.98 and 0.02, respectively (Figure 1c). In the CCBN experiment, the interannual and seasonal changes in MARS's Alk and DIC were removed, but the MARS's Alk:DIC ratio did not depart significantly from the average hindcast value. The CCBN experiment then modified the relationship between discharge and both coastal Alk and DIC, but it did not change much the relationship between discharge and the coastal Alk:DIC ratio. Thus, the balance between coastal Alk and DIC was very similar (Figures S8e and S9e in Supporting Information S1). Changes in the MARS's Alk:DIC ratio did produce changes in the interannual Ω_{Ar} anomalies. In the Alk90 experiment, where the ratio was decreased by 10%, the significant positive $sf\Omega_{Ar}$ anomalies vanished (Figure 7c). On the other hand, the Alk110 experiment, whose ratio was increased by 10%, displayed a significant strengthening of the positive $sf\Omega_{Ar}$ anomalies, with an average increase over the central inner-shelf ranging from 0.05 in spring to 0.12 in summer (Figure 7d). Changes in MARS nitrate concentration also impacted the interannual Ω_{Ar} variability, especially in summer. A nitrate reduction of 20% and 50%, as in the N80 and N50 experiments, led to a corresponding mean decrease of 0.05 and 0.13 units in the $sf\Omega_{Ar}$anomalies during summer (Figures 7e and 7f), concurrent with average reductions of 10% and 25% in the surface NCP anomaly over the central inner shelf (not shown), which suppressed the positive $sf\Omega_{Ar}$ anomalies.

To further illustrate the system responses to interannual river runoff variability in the hindcast, CCBN, and N50 experiments, we conducted a correlation analysis between MARS discharge and simulated carbonate system variables around the MARS delta at surface, spatially averaged from 93° to 90°W and northward of 28.5°N, a region directly impacted by the MARS outflows. We exclude from the spatial averaging locations with salinity below 20, where the phytoplankton response to riverine nutrient was strongly light-limited. This usually corresponded to a few data points near the Mississippi and Atchafalaya mouths. As in the composites analysis, a 1-week lag was considered between series to derive the correlations. Consistent with the composite's results, the correlation patterns for *sf*Alk and *sf*DIC showed important differences between the hindcast and CCBN

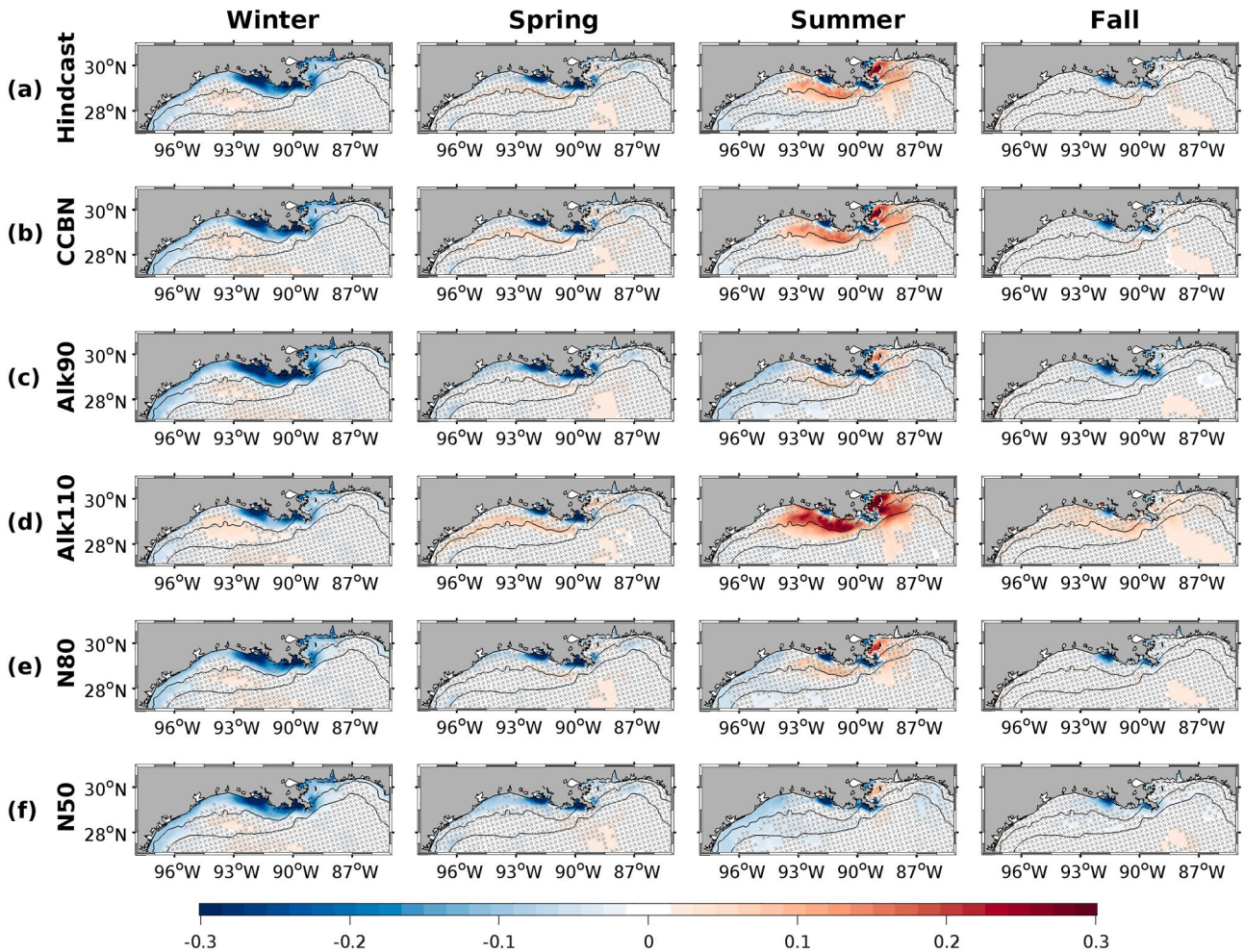

Figure 7. High discharge composites of the mean surface Ω_{Ar} anomaly derived from the following experiments: (a) Hindcast, (b) Constant carbonate (CCBN), (c) Alkalinity 90% (Alk90), (d) Alkalinity 110% (Alk110), (e) Nitrate 80% (N80), and (f) Nitrate 50% (N50). Anomaly series were detrended before estimating the composites. Black contours depict the 25 and 200 m isobaths. Gray slash pattern represents non-significant values.

experiments (Figures 8a and 8b), while the correlation between discharge and the surface Alk:DIC ratio was very similar between the two experiments (Figure 8c). It is worth noting that under conservative mixing, we would expect a negative correlation between discharge and the Alk:DIC ratio near the delta year-round, since the average MARS ratio was always smaller than the surface ocean ratio (~0.98 vs. 1.18). Consequently, the positive correlation coefficients obtained during summer mainly reflect biological uptake of DIC counteracting the low ratio signature from the MARS waters (Figure 8c). Biology also explains the strong seasonality in the discharge-*sf*DIC correlation of the CCBN experiment, with significant positive correlation in winter and significant negative correlation in summer, something not evident in the hindcast *sf*DIC, as the latter was also modulated by the river DIC seasonality. In the N50 experiment, the correlation patterns for *sf*Alk and *sf*DIC were similar to the hindcast patterns, but the decreased biological uptake, linked to decreased riverine nutrient, led to a weaker phytoplankton impact on the Alk:DIC ratio during summer (Figure 8c). Since Ω_{Ar} is modulated by the Alk:DIC ratio, the discharge-Ω_{Ar} correlation pattern showed significant negative coefficients in winter for the three experiments, and significant positive coefficients in summer for the hindcast and CCBN experiments (Figure 8d).

3.3. Ω_{Ar} Frequency Distribution

The MARS-induced Ω_{Ar} anomalies described above implied changes in the probability distribution function of Ω_{Ar} nearshore, which has the potential for a significant impact in calcifying organisms. To evaluate this, we derived frequency histograms for $sf\Omega_{Ar}$ and $b\Omega_{Ar}$, from the hindcast and quantified the fraction of suboptimal

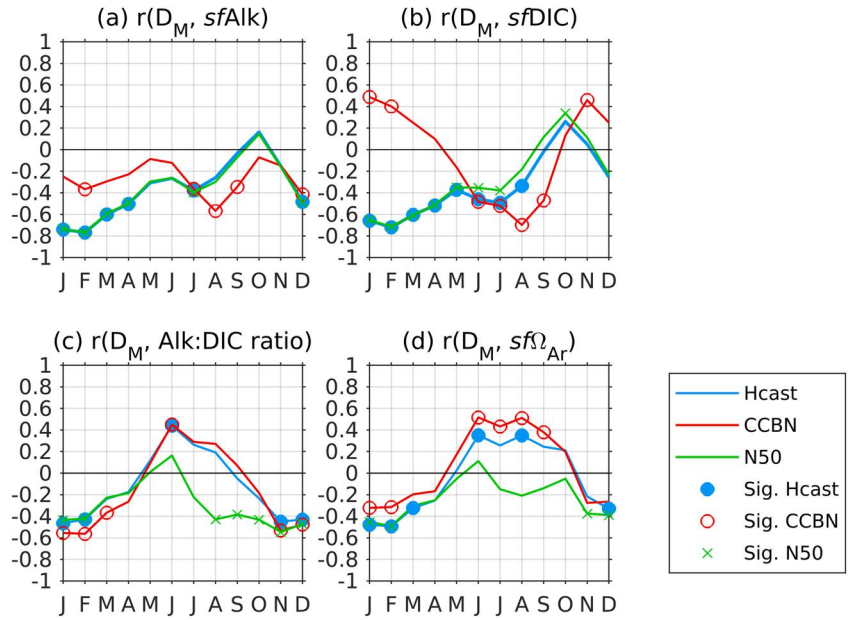

Figure 8. Monthly correlation coefficients between MARS discharge (D_M) and simulated spatially averaged series of surface alkalinity (*sf*Alk), surface dissolved inorganic carbon (*sf*DIC), surface alkalinity to DIC ratio (Alk:DIC ratio), and surface aragonite saturation ($sf\Omega_{Ar}$) over 93°–90°W and north of 28.0°N, as derived from the hindcast (Hcast), Constant Carbonate (CCBN), and Nitrate 50% (N50) experiments. Carbon system variables were derived for locations with surface salinities greater than 20. A 1-week lag was considered between series (discharge leading). All series were detrended before correlation.

values ($\Omega_{Ar} < 2$), over the inner shelf region near the delta under high and low MARS discharge. To limit the impact of OA and other low-frequency related changes in our calculations, independent estimates of histograms and suboptimal fractions were derived for 1980–1999 and 2000–2019. We present below the patterns for the latter period, but similar results were obtained for the former period (Table S3 and Figure S10 in Supporting Information S1). The derived Ω_{Ar} histograms for 2000–2019 showed significant differences between discharge scenarios, seasons, and vertical layers (Figure 9). Enhanced MARS discharge increased the suboptimal fraction in all seasons. This is reflected in the ratio between the suboptimal Ω_{Ar} fraction under high and low discharge conditions. At surface, that ratio was 4.4, 2.4, 4.0, and 21.0 during winter, spring, summer, and fall, respectively. At bottom, the same ratio was 4.2, 2.0, 6.2, and 5.0, respectively. The greatest portion of suboptimal $sf\Omega_{Ar}$ values was 14.6% in winter, and the greatest portion of suboptimal $b\Omega_{Ar}$ was 32.8% in summer. Moreover, during high discharge spring and summers, 2.6% and 7.4% of the $b\Omega_{Ar}$ values were below one, which represents corrosive conditions for aragonite. Suboptimal Ω_{Ar} conditions were infrequent in fall, corresponding to less than 3% of the outputs under high discharge.

We also calculated the suboptimal Ω_{Ar} fractions for our five sensitivity experiments (Table S4 in Supporting Information S1). As expected from the previous results, the more meaningful differences from the hindcast were associated with the Alk90, Alk110, N80, and N50 experiments. Alk90 promoted about 50% increase in the suboptimal surface fraction during high-discharge winters and springs, and about 20% increase in the suboptimal bottom fraction during high-discharge summers, whereas Alk110 produced the opposite effects. In the case of the N80 and N50 experiments, the main differences from the hindcast were obtained at bottom during high-discharge summers, where the suboptimal fraction decreased by about 20% and 50%, respectively.

4. Discussion

A composite analysis of simulated carbonate system variables was conducted to describe emerging anomaly patterns under high and low MARS discharge years. Our motivation was to examine the impacts of river carbonate chemistry and nutrient runoff on the interannual Ω_{Ar} variability. The model results showed an important seasonal variation in the relevance of these two driving mechanisms. High discharge winters promoted negative $sf\Omega_{Ar}$ and $b\Omega_{Ar}$ anomalies near the MARS delta, mainly driven by the mixing of MARS waters with a low Alk:

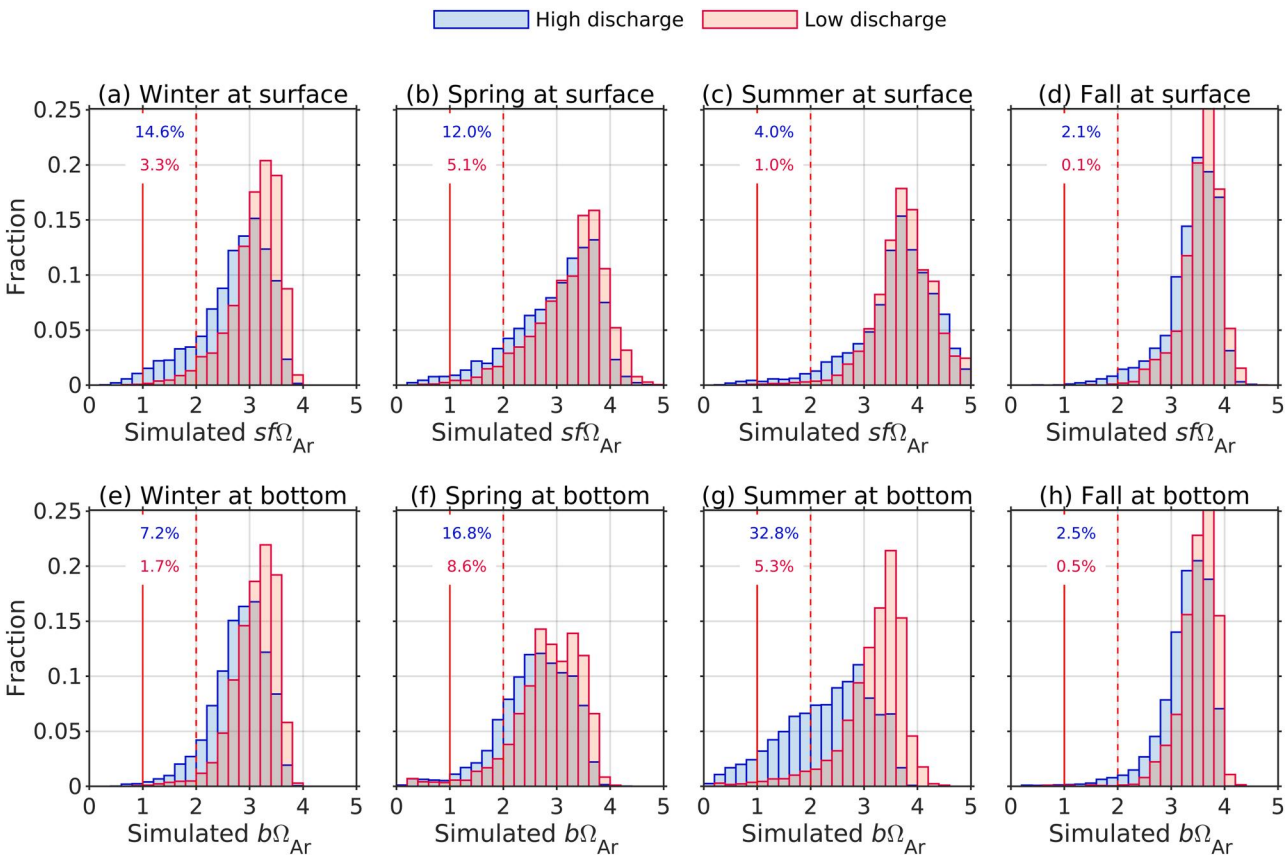

Figure 9. Frequency histograms for the simulated surface (a–d) and bottom (e–h) aragonite saturation state over the central part of the northern Gulf inner shelf (<25 m bottom depth; 93°–89°W) during the high and low discharge conditions from 2000 to 2019: (a, e) winter, (b, f) spring, (c, g) summer, and (d–h) fall. Blue and red numbers at each panel indicate the percentage of suboptimal values ($\Omega_{Ar} < 2$) during high and low discharge, respectively.

DIC ratio. High discharge summers promoted strong negative $b\Omega_{Ar}$ anomalies and less intense but significant positive $sf\Omega_{Ar}$ anomalies, which were mainly associated with biological-changes fostered by nutrient runoff and salinity-driven stratification. Previous studies in the northern GoM showed that biological processes play an important role in the generation of bottom acidification (e.g., Cai et al., 2011), and that the interaction between MARS carbonate chemistry and biology influenced the spatial variability in surface Ω_{Ar} (e.g., Guo et al., 2012; Huang et al., 2021). Our results are consistent with those studies, providing an extended framework that includes discharge, the Alk:DIC ratio, and nutrients from the MARS as main parameters to understand interannual patterns in the coastal carbonate system.

Our analysis of the USGS-derived river chemistry revealed an important temporal variability in Alk and DIC from the MARS, which is inversely related to river discharge. This flow-dependent pattern is a common feature in many riverine systems, associated with the dilution of major river's solutes during high-discharge periods (Gomez et al., 2023; Joesoef et al., 2017; Li et al., 2022). The seasonal changes in MARS's carbonate chemistry decreased both Alk and DIC during winter-spring, and increased it during summer-fall. The flow-dependent interannual anomalies in river Alk and river DIC reinforced the coastal dilution effect during high-discharge winters and springs, producing significant negative anomalies in *sf*Alk, *b*Alk, and *sf*DIC over the inner-shelf. However, since Alk and DIC from the MARS were highly correlated ($r = 0.99$), the MARS's Alk:DIC ratio displayed a rather weak seasonal and interannual variability, which was also unrelated to the river flow changes. The average MARS's Alk:DIC ratio was about 17% lower than the surface open GoM values, which implies that the freshwater contributed to decreasing the surface Ω_{Ar} values near the delta year-round, despite the relatively high alkalinity values in the Mississippi River, greater than the ocean alkalinity values during summer-fall.

Sensitivity analysis revealed that the interannual Ω_{Ar} anomalies are more responsive to changes in the river Alk:DIC ratio than the seasonal changes in the magnitude of the river Alk and river DIC concentrations. This is

because the effect of Alk and DIC on Ω_{Ar} counteracted each other; thus, the total Ω_{Ar} anomaly is largely determined by a small residual difference between the two drivers. The low river Alk:DIC ratio is to some degree offset by enhanced biological uptake at surface fostered by MARS's nutrient runoff. High-discharge conditions increase surface NCP during the four seasons, but significant positive $sf\Omega_{Ar}$ anomalies were only obtained in summer, concurrent with the largest negative anomalies in $b\Omega_{Ar}$. This last pattern is linked to the strong salinity-driven vertical stratification, which promotes a decoupling between phytoplankton production in the upper layer and respiration below (Cai et al., 2011; Laurent et al., 2017). The interannual Ω_{Ar} patterns are sensitive to changes in nitrate content, with decreased nitrate values lessening or even reversing the positive $sf\Omega_{Ar}$ anomalies during high-discharge summers. Our result adds to a previous modeling study by Xue et al. (2016), which explored carbon system sensitivity to changes in MARS chemistry, but focused on CO_2 patterns. Consistent with our results, they found that an enhanced concentration in river nitrate led to increased biological uptake of DIC near the delta, reflected in reduced surface pCO_2 levels.

The northern GoM shelf is a region characterized by a large spatiotemporal variability in carbonate system variables, which added to the still limited length of observational records make it difficult to discern interannual variation from long-term trend in pH, pCO_2, or Ω_{Ar} (e.g., Kealoha et al., 2020). Thus, the interannual variability and its modulation by the MARS runoff have remained poorly documented, implying an important gap that limits our ability to quantify the northern GoM ecosystem vulnerability to OA progression and other stressors. Our model results suggest a greater prevalence of suboptimal Ω_{Ar} values near the MARS delta under high-discharge periods. As bottom acidification is a seasonally recurring phenomena, the greatest suboptimal Ω_{Ar} fraction near the bottom was obtained under high-discharge summers, representing about one-third of the inner-shelf values near the MARS delta. Suboptimal conditions were also simulated in the surface layer, especially under high-discharge winters, representing about 15% of the inner-shelf values during 2000–2019. In comparison, the corresponding suboptimal values under low-discharge summers and winters were 5% and 3%, respectively. This indicates an enhanced vulnerability of calcifying organisms under flooding conditions, which are expected to increase their frequency due to climate change (Hicks et al., 2022; Tao et al., 2014). Our sensitivity experiments revealed significant changes in the suboptimal Ω_{Ar} fractions associated with minor variations in river alkalinity (representing $\pm$10% variations in the river Alk:DIC ratio) and reduction in river nitrate. In addition, a 50% reduction in river nitrate led to a 50% decrease in the suboptimal bottom Ω_{Ar} fraction on the inner-shelf near the MARS delta. This result highlights the relevance of the efforts by the Hypoxia Task Force to reduce nitrogen pollution in the MARS. Further studies are needed to investigate river-induced disturbances of the coastal carbonate system and to improve the still limited understanding of the species tolerance to low Ω_{Ar} and pH levels in the region (Osborne et al., 2022), so that suitable strategies for the management of marine resources can be developed.

Our findings contribute to an increasing number of regional modeling studies showing that river runoff plays a key role as driver of carbonate variability in river influenced ocean margins (e.g., Moore-Maley et al., 2018; Shen et al., 2020; Siedlecki et al., 2017; Xue et al., 2016). In the northern GoM shelf, river inputs are largely dominated by the MARS signature, but small rivers can also play a significant role as drivers of Ω_{Ar} variability at a more local level (estuaries, bays). The system could be especially sensitive to rivers along the states of Mississippi and Alabama (east of the MARS delta), as those are characterized by much lower Alk:DIC ratios than the MARS (Gomez et al., 2023), which would negatively impact Ω_{Ar}. It has been shown that El Nino-Southern Oscillation (ENSO) influences the MARS discharge during winter, as well as discharges from other northern GoM rivers during winter-spring, with El Niño periods associated with increased river flow and La Niña periods with decreased river flow (e.g., Gomez et al., 2019; Tootle et al., 2005). Consistently, our selected high (low) discharge winters for the composite analysis coincide with El Nino (La Nina) periods during 2000–2019. This opens a potential for seasonal predictability of the carbonate system disturbances in the northern GoM shelf, which deserves further attention.

Finally, multiple studies showed a prevailing pattern of increased alkalinity concentration in U.S. rivers during the last decades, including the MARS (e.g., Stets et al., 2014). This long-term alkalinity increase has been related to agriculture disturbances, such as changes in water fluxes and soil liming (e.g., Kaushal et al., 2013; Raymond et al., 2008; Stets et al., 2014), as well as management efforts to reduce water pollution (Turner, 2021). USGS records shows that the average alkalinity and DIC concentration in the Mississippi river rose about 15% and 10% from 1970–1979 to 2010–2019, respectively, which led to a 5% increase in the Alk:DIC ratio. It is worth noting that since we were focused in examining interannual Ω_{Ar} patterns, our composites were derived from detrended

model anomalies. Thus, we removed the signal linked to multidecadal changes in MARS chemistry. However, the modeling study by Gomez et al. (2021) showed that the long-term alkalinization experienced by the MARS has a significant impact on OA progression. In light of the present study results, we could indicate that rather than the change in river alkalinity it was the change in the river Alk:DIC ratio that mainly drove that slowdown in OA progression. We also emphasizes that the MARS waters do not have a direct positive effect on Ω_{Ar}, as the MARS Alk:DIC ratio is smaller than the surface open ocean ratio. However, a recovery in water quality of the MARS during recent decades (Turner, 2021), reflected in an increased river Alk:DIC ratio, ameliorated its negative impact on the buffer capacity near the delta, slowing down the long-term decline in Ω_{Ar}.

5. Conclusions

Based on model results, we showed that interannual changes in MARS discharge impact the carbonate system in the northern GoM inner-shelf, inducing significant Ω_{Ar} anomalies. Those changes are mainly driven by the mixing of river waters with a low Alk:DIC ratio, and increased biological production stimulated by the associated riverine nutrient input. The impact of the low buffer capacity on Ω_{Ar} is more pronounced during winter, while the impact of biologically driven processes is more important in summer. Sensitivity experiments suggested that the MARS's Alk:DIC ratio and nitrate concentration are key parameters influencing interannual coastal carbonate variability in the northern GoM shelf. High discharge conditions increased the simulated fraction of coastal waters with Ω_{Ar} levels below two, thus increasing the vulnerability of calcifying organisms to OA.

Data Availability Statement

The model outputs used in this study can be found at the NOAA National Center for Environmental Information repository via https://www.ncei.noaa.gov/archive/accession/0277155. The ERA5 reanalysis product, the river chemistry data, and river discharge data were obtained at https://www.ecmwf.int/en/forecasts/dataset/ecmwf-reanalysis-v5, https://doi.org/10.25921/9jfw-ph50, and https://geo.gcoos.org/river_discharge, respectively.

Acknowledgments
This article was supported by the NOAA Ocean Acidification Program, NOAA Climate Program Office, and NOAA Atlantic Oceanographic and Meteorological Laboratory. The research was conducted under NOAA's award NA21OAR4320190 to the Northern Gulf Institute.

References

Cai, W. J., Hu, X., Huang, W. J., Murrell, M. C., Lehrter, J. C., Lohrenz, S. E., et al. (2011). Acidification of subsurface coastal waters enhanced by eutrophication. *Nature Geoscience*, *4*(11), 766–770. https://doi.org/10.1038/ngeo1297

Dickson, A. G. (1990). Thermodynamics of the dissociation of boric acid in synthetic seawater from 273.15 to 318.15 K. *Deep-Sea Research, Part A: Oceanographic Research Papers*, *37*(5), 755–766. https://doi.org/10.1016/0198-0149(90)90004-F

Doney, S. C., Fabry, V. J., Feely, R. A., & Kleypas, J. A. (2009). Ocean acidification: The other CO_2 problem. *Annual Review of Marine Science*, *1*, 169–192. https://doi.org/10.1146/annurev.marine.010908.163834

Duarte, C. M., Hendriks, I. E., Moore, T. S., Olsen, Y. S., Steckbauer, A., Ramajo, L., et al. (2013). Is ocean acidification an open-ocean syndrome? Understanding anthropogenic impacts on seawater pH. *Estuaries and Coasts*, *36*(2), 221–236. https://doi.org/10.1007/s12237-013-9594-3

Gomez, F. A., Lee, S. K., Hernandez, F. J., Jr., Chiaverano, L. M., Muller-Karger, F. E., Liu, Y., & Lamkin, J. T. (2019). ENSO-induced co-variability of salinity, plankton biomass and coastal currents in the northern Gulf of Mexico. *Scientific Reports*, *9*(1), 178. https://doi.org/10.1038/s41598-018-36655-y

Gomez, F. A., Lee, S.-K., Stock, C. A., Ross, A. C., Resplandy, L., Siedlecki, S. A., et al. (2023). RC4USCoast: A river chemistry dataset for regional ocean model applications in the US East Coast, Gulf of Mexico, and US west coast. *Earth System Science Data*, *15*(5), 2223–2234. https://doi.org/10.5194/essd-15-2223-2023

Gomez, F. A., Wanninkhof, R., Barbero, L., & Lee, S.-K. (2021). Increasing river alkalinity slows ocean acidification in the northern Gulf of Mexico. *Geophysical Research Letters*, *48*(24), e2021GL096521. https://doi.org/10.1029/2021GL096521

Gomez, F. A., Wanninkhof, R., Barbero, L., Lee, S. K., & Hernandez, F. J. (2020). Seasonal patterns of surface inorganic carbon system variables in the Gulf of Mexico inferred from a regional high-resolution ocean biogeochemical model. *Biogeosciences*, *17*(6), 1685–1700. https://doi.org/10.5194/bg-17-1685-2020

Gruber, N., Clement, D., Carter, B. R., Feely, R. A., Van Heuven, S., Hoppema, M., et al. (2019). The oceanic sink for anthropogenic CO_2 from 1994 to 2007. *Science*, *363*(6432), 1193–1199. https://doi.org/10.1126/science.aau5153

Guo, X., Cai, W. J., Huang, W. J., Wang, Y., Chen, F., Murrell, M. C., et al. (2012). Carbon dynamics and community production in the Mississippi River plume. *Limnology & Oceanography*, *57*(1), 1–17. https://doi.org/10.4319/lo.2012.57.1.0001

Hersbach, H., Bell, B., Berrisford, P., Hirahara, S., Horányi, A., Muñoz-Sabater, J., et al. (2020). The ERA5 global reanalysis. *Quarterly Journal of the Royal Meteorological Society*, *146*(730), 1999–2049. https://doi.org/10.1002/qj.3803

Hicks, T. L., Shamberger, K. E. F., Fitzsimmons, J. N., Jensen, C. C., & DiMarco, S. F. (2022). Tropical cyclone-induced coastal acidification in Galveston Bay, Texas. *Communications Earth & Environment*, *3*(1), 297. https://doi.org/10.1038/s43247-022-00608-1

Huang, W. J., Cai, W. J., & Hu, X. (2021). Seasonal mixing and biological controls of the carbonate system in a riverriver-dominated continental shelf subject to eutrophication and hypoxia in the northern Gulf of Mexico. *Frontiers in Marine Science*, *8*, 621243. https://doi.org/10.3389/fmars.2021.621243

Huang, W. J., Cai, W. J., Wang, Y., Lohrenz, S. E., & Murrell, M. C. (2015). The carbon dioxide system on the Mississippi River-dominated continental shelf in the northern Gulf of Mexico: 1. Distribution and air-sea CO_2 flux. *Journal of Geophysical Research: Oceans*, *120*(3), 1429–1445. https://doi.org/10.1002/2014JC010498

Joesoef, A., Kirchman, D. L., Sommerfield, C. K., & Cai, W.-J. (2017). Seasonal variability of the inorganic carbon system in a large coastal plain estuary. *Biogeosciences*, *14*(21), 4949–4963. https://doi.org/10.5194/bg-14-4949-2017

Kaushal, S. S., Likens, G. E., Utz, R. M., Pace, M. L., Grese, M., & Yepsen, M. (2013). Increased river alkalinization in the Eastern US. *Environmental Science and Technology*, *47*(18), 10302–10311. https://doi.org/10.1021/es401046s

Kealoha, A. K., Shamberger, K. E., DiMarco, S. F., Thyng, K. M., Hetland, R. D., Manzello, D. P., et al. (2020). Surface water CO_2 variability in the Gulf of Mexico (1996–2017). *Scientific Reports*, *10*(1), 1–13. https://doi.org/10.1038/s41598-020-68924-0

Kekuewa, S. A. H., Courtney, T. A., Cyronak, T., & Andersson, A. J. (2022). Seasonal nearshore ocean acidification and deoxygenation in the Southern California Bight. *Scientific Reports*, *12*(1), 17969. https://doi.org/10.1038/s41598-022-21831-y

Lacroix, F., Ilyina, T., & Hartmann, J. (2020). Oceanic CO_2 outgassing and biological production hotspots induced by pre-industrial river loads of nutrients and carbon in a global modelling approach. *Biogeosciences*, *17*(1), 55–88. https://doi.org/10.5194/bg-17-55-2020

Lacroix, F., Ilyina, T., Mathis, M., Laruelle, G. G., & Regnier, P. (2021). Historical increases in land-derived nutrient inputs may alleviate effects of a changing physical climate on the oceanic carbon cycle. *Global Change Biology*, *27*(21), 5491–5513. https://doi.org/10.1111/gcb.15822

Laurent, A., Fennel, K., Cai, W.-J., Huang, W.-J., Barbero, L., & Wanninkhof, R. (2017). Eutrophication-induced acidification of coastal waters in the northern Gulf of Mexico: Insights into origin and processes from a coupled physical-biogeochemical model. *Geophysical Research Letters*, *44*(2), 946–956. https://doi.org/10.1002/2016GL071881

Li, L., Stewart, B., Zhi, W., Sadayappan, K., Ramesh, S., Kerins, D., et al. (2022). Climate controls on river chemistry. *Earth's Future*, *10*(6), e2021EF002603. https://doi.org/10.1029/2021EF002603

Liu, X., Stock, C. A., Dunne, J. P., Lee, M., Shevliakova, E., Malyshev, S., & Milly, P. C. (2021). Simulated global coastal ecosystem responses to a half-century increase in river nitrogen loads. *Geophysical Research Letters*, *48*(17), e2021GL094367. https://doi.org/10.1029/2021GL094367

Liu, Y., Lee, S. K., Enfield, D. B., Muhling, B. A., Lamkin, J. T., Muller-Karger, F. E., & Roffer, M. A. (2015). Potential impact of climate change on the Intra-Americas Sea: Part-1: A dynamic downscaling of the CMIP5 model projections. *Journal of Marine Systems*, *148*, 56–69. https://doi.org/10.1016/j.jmarsys.2015.01.007

Lohrenz, S. E., & Cai, W. J. (2006). Satellite ocean color assessment of air-sea fluxes of CO_2 in a river-dominated coastal margin. *Geophysical Research Letters*, *33*(1), L01601. https://doi.org/10.1029/2005GL023942

Martínez-López, B., & Zavala-Hidalgo, J. (2009). Seasonal and interannual variability of cross-shelf transports of chlorophyll in the Gulf of Mexico. *Journal of Marine Systems*, *77*(1–2), 1–20. https://doi.org/10.1016/j.jmarsys.2008.10.002

Millero, F. J. (2010). Carbonate constants for estuarine waters. *Marine and Freshwater Research*, *61*(2), 139–142. https://doi.org/10.1071/MF09254

Moore-Maley, B. L., Ianson, D., & Allen, S. E. (2018). The sensitivity of estuarine aragonite saturation state and pH to the carbonate chemistry of a freshet-dominated river. *Biogeosciences*, *15*(12), 3743–3760. https://doi.org/10.5194/bg-15-3743-2018

Muñoz-Salinas, E., & Castillo, M. (2015). Streamflow and sediment load assessment from 1950 to 2006 in the Usumacinta and Grijalva rivers (Southern Mexico) and the influence of ENSO. *Catena*, *127*, 270–278. https://doi.org/10.1016/j.catena.2015.01.007

Orr, J., Fabry, V., Aumont, O., Bopp, L., Doney, S. C., Feely, R. A., et al. (2005). Anthropogenic ocean acidification over the twenty-first century and its impact on calcifying organisms. *Nature*, *437*(7059), 681–686. https://doi.org/10.1038/nature04095

Osborne, E., Hu, X., Hall, E. R., Yates, K., Vreeland-Dawson, J., Shamberger, K., et al. (2022). Ocean acidification in the Gulf of Mexico: Drivers, impacts, and unknowns. *Progress in Oceanography*, *209*, 102882. https://doi.org/10.1016/j.pocean.2022.102882

Rabalais, N. N., Turner, R. E., Sen Gupta, B. K., Boesch, D. F., Chapman, P., & Murrell, M. C. (2007). Hypoxia in the northern Gulf of Mexico: Does the science support the plan to reduce, mitigate, and control hypoxia? *Estuaries and Coasts*, *30*(5), 753–772. https://doi.org/10.1007/BF02841332

Raymond, P. A., Oh, N. H., Turner, R. E., & Broussard, W. (2008). Anthropogenically enhanced fluxes of water and carbon from the Mississippi River. *Nature*, *451*(7177), 449–452. https://doi.org/10.1038/nature06505

Regnier, P., Resplandy, L., Najjar, R. G., & Ciais, P. (2022). The land-to-ocean loops of the global carbon cycle. *Nature*, *603*(7901), 401–410. https://doi.org/10.1038/s41586-021-04339-9

Shchepetkin, A. F., & McWilliams, J. C. (2005). The regional oceanic modeling system (ROMS): A split-explicit, free-surface, topography-following-coordinate oceanic model. *Ocean Modelling*, *9*(4), 347–404. https://doi.org/10.1016/j.ocemod.2004.08.002

Shen, C., Testa, J. M., Li, M., & Cai, W.-J. (2020). Understanding anthropogenic impacts on pH and aragonite saturation state in Chesapeake Bay: Insights from a 30-year model study. *Journal of Geophysical Research: Biogeosciences*, *125*(7), e2019JG005620. https://doi.org/10.1029/2019JG005620

Siedlecki, S. A., Pilcher, D. J., Hermann, A. J., Coyle, K., & Mathis, J. (2017). The importance of freshwater to spatial variability of aragonite saturation state in the Gulf of Alaska. *Journal of Geophysical Research: Oceans*, *122*(11), 8482–8502. https://doi.org/10.1002/2017JC012791

Siedlecki, S. A., Salisbury, J., Gledhill, D. K., Bastidas, C., Meseck, S., McGarry, K., et al. (2021). Projecting ocean acidification impacts for the Gulf of Maine to 2050: New tools and expectations. *Elementa: Science of the Anthropocene*, *9*(1), 00062. https://doi.org/10.1525/elementa.2020.00062

Stets, E. G., Kelly, V. J., & Crawford, C. G. (2014). Long-term trends in alkalinity in large rivers of the conterminous US in relation to acidification, agriculture, and hydrologic modification. *Science of the Total Environment*, *488*, 280–289. https://doi.org/10.1016/j.scitotenv.2014.04.054

Tao, B., Tian, H., Ren, W., Yang, J., Yang, Q., He, R., et al. (2014). Increasing Mississippi river discharge throughout the 21st century influenced by changes in climate, land use, and atmospheric CO_2. *Geophysical Research Letters*, *41*(14), 4978–4986. https://doi.org/10.1002/2014GL060361

Tootle, G. A., Piechota, T. C., & Singh, A. (2005). Coupled oceanic-atmospheric variability and US streamflow. *Water Resources Research*, *41*(12), W12408. https://doi.org/10.1029/2005WR004381

Turner, R. E. (2006). Will lowering estuarine salinity increase Gulf of Mexico oyster landings? *Estuaries and Coasts*, *29*(3), 345–352. https://doi.org/10.1007/BF02784984

Turner, R. E. (2021). Declining bacteria, lead, and sulphate, and rising pH and oxygen in the lower Mississippi River. *Ambio*, *50*(9), 1–1738. https://doi.org/10.1007/s13280-020-01499-2

van Heuven, S. M. A. C., Pierrot, D., Rae, J. W. B., Lewis, E., & Wallace, D. W. R. (2011). MATLAB program developed for CO_2 system calculations. In *ORNL/CDIAC-105b. Carbon dioxide information analysis center* (Vol. 530). Oak Ridge National Laboratory, US Department of Energy. https://doi.org/10.3334/CDIAC/otg.CO2SYS_MATLAB_v1.1

von Storch, H., & Zwiers, F. W. (1999). *Statistical analysis in climate research* (p. 484). Cambridge University Press. https://doi.org/10.1017/CBO9780511612336

Wang, Z. A., Wanninkhof, R., Cai, W. J., Byrne, R. H., Hu, X., Peng, T. H., & Huang, W. J. (2013). The marine inorganic carbon system along the Gulf of Mexico and Atlantic coasts of the United States: Insights from a transregional coastal carbon study. *Limnology and Oceanography*, *58*(1), 325–342. https://doi.org/10.4319/lo.2013.58.1.0325

Wanninkhof, R., Barbero, L., Byrne, R., Cai, W. J., Huang, W. J., Zhang, J. Z., et al. (2015). Ocean Acidification along the Gulf coast and east Coast of the USA. *Continental Shelf Research*, *98*, 54–71. https://doi.org/10.1016/j.csr.2015.02.008

Weiss, R. (1974). Carbon dioxide in water and seawater: The solubility of a non-ideal gas. *Marine Chemistry*, *2*(3), 203–215. https://doi.org/10.1016/0304-4203(74)90015-2

Xue, Z., He, R., Fennel, K., Cai, W.-J., Lohrenz, S., Huang, W.-J., et al. (2016). Modeling pCO_2 variability in the Gulf of Mexico. *Biogeosciences*, *13*(15), 4359–4377. https://doi.org/10.5194/bg-13-4359-2016

Yang, B., Byrne, R. H., & Wanninkhof, R. (2015). Subannual variability of total alkalinity distributions in the northeastern Gulf of Mexico. *Journal of Geophysical Research: Oceans*, *120*(5), 3805–3816. https://doi.org/10.1002/2015JC010780